NANO LETTERS

pubs.acs.org/NanoLett Letter

Wafer-Scale Programmed Assembly of One-Atom-Thick Crystals

Seong-Jun Yang,[⊥] Ju-Hyun Jung,[⊥] Eunsook Lee, Edmund Han, Min-Yeong Choi, Daesung Jung, Shinyoung Choi, Jun-Ho Park, Dongseok Oh, Siwoo Noh, Ki-Jeong Kim, Pinshane Y. Huang, Chan-Cuk Hwang, and Cheol-Joo Kim*

Cite This: https://doi.org/10.1021/acs.nanolett.1c04139 Read Online

ACCESS | Metrics & More | Article Recommendations | Supporting Information

ABSTRACT: Crystalline films offer various physical properties based on the modulation of their thicknesses and atomic structures. The layer-by-layer assembly of atomically thin crystals provides a powerful means to arbitrarily design films at the atomic level, which are unattainable with existing growth technologies. However, atomically clean assembly of the materials with high scalability and reproducibility remains challenging. We report programmed crystal assembly of graphene and monolayer hexagonal boron nitride, assisted by van der Waals interactions, to form wafer-scale films of pristine interfaces with near-unity yield. The atomic configurations of the films are tailored with layer-resolved compositions and in-plane crystalline orientations. We demonstrate batch-fabricated tunnel device arrays with modulation of the resistance over orders of magnitude by thickness control of the hexagonal boron nitride barrier with single-atom precision and large-scale, twisted multilayer graphene with programmable electronic band structures and crystal symmetries. Our results constitute an important development in the artificial design of large-scale films.

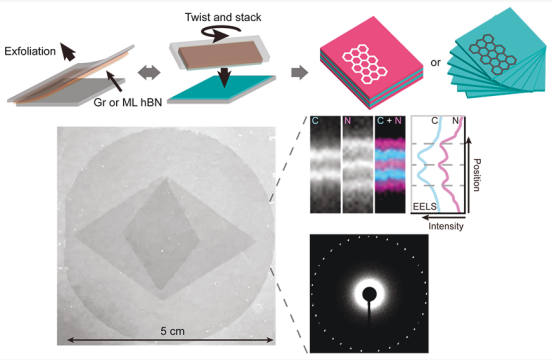

KEYWORDS: *graphene, hexagonal boron nitride, twisted graphene, van der Waals heterostructures, layer-by-layer assembly, two dimensional materials, tunnel device*

Since the reports of various two-dimensional (2D) materials after the isolation of graphene, the assembly of these materials into artificial structures has been intensely studied for discovery of novel properties and fabrication of advanced nanodevices.[1] The assembly of 2D materials provides a variety of van der Waals structures by structural degrees of freedom that are difficult to achieve with conventional deposition techniques of bulk materials or thin films that exploit self-assembly processes and has two unique advantages. First, the separation of the growth and assembly steps enables various combinations of materials that have incompatible growth conditions.[2,3] Second, the absence of chemical bonds between adjacent layers allows for control of the crystalline orientation of individual layers to modulate the atomic configurations of the whole structure.[4,5] Therefore, even with small varieties of 2D materials, numerous multilayer structures have been fabricated to host programmed interactions with various fundamental particles, including electrons,[6−8] ions,[9] phonons,[10] and polaritons.[11]

Graphene and hBN form the key assembly units with unique electrical, optical, and mechanical properties. Mechanical assembly of 2D materials, assisted by van der Waals interactions[2,12,13] produces pristine, controlled interfaces through which the properties of final stacks are programmed. However, current mechanical methods to assemble graphene and hBN have low throughput, due to the lack of reliable production of uniform assembly units. They are obtained by either exfoliating flakes from bulk crystals or using chemical vapor deposition (CVD) to grow films. Exfoliated flakes have spatially nonuniform thickness and small sizes, typically on the scale of tens of micrometers, limited by the size of bulk crystals.[12,13] Epitaxial growth by CVD produces wafer-scale films with aligned crystallinity,[14,15] but the conventional process to assemble the films involves wet-process, which induces interfacial contaminants.[16] In the past few years, there has been rapid progress in the assembly of large-scale transition metal dichalcogenides;[2] however, atomically clean assembly of graphene and hBN crystals is still elusive and remains a key technique to be developed (see Supporting Information and Figure S1). The reliable assembly of graphene and hBN with atomic-level precision would enable fabrication of high-quality, van der Waals structures with greatly extended tunability.

Received: October 26, 2021
Revised: January 25, 2022

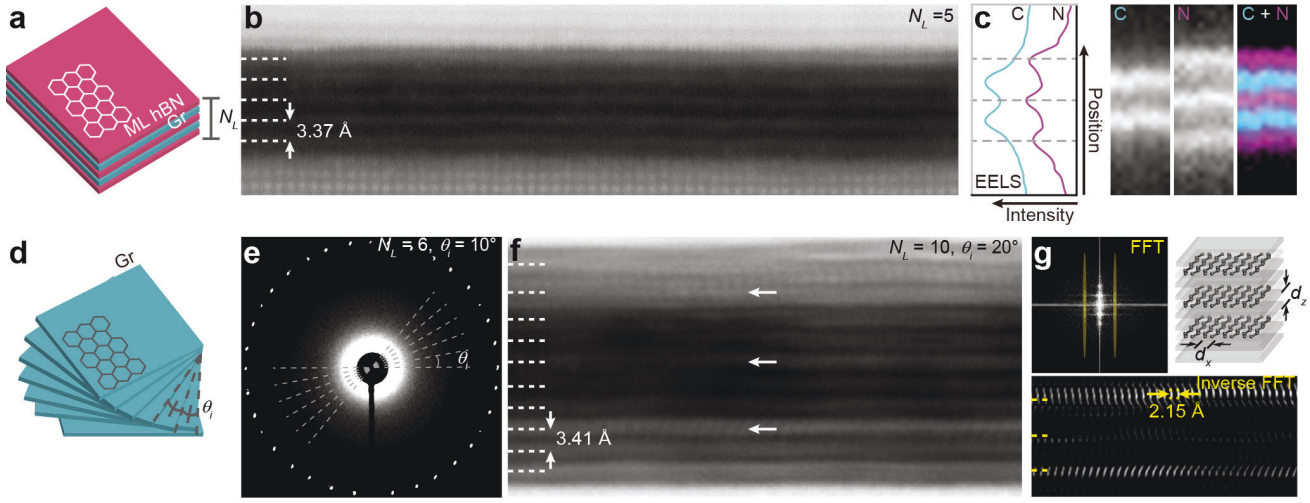

Figure 1. Artificial van der Waals films with high-quality interfaces. (a) Schematic of graphene/hBN vertical superlattice. (b) Annular dark-field STEM image of a cross section of the graphene/hBN vertical superlattice (N_L = 5). (c) EELS intensity profiles and composition maps along out-of-plane direction. The apparent curvatures of layers in the EELS maps are a result of specimen drift during acquisition rather than real sample roughness. (d) Schematic of CTG. (e) TEM diffraction pattern from a top view of a CTG (N_L = 6, θ_i = 10°) that is measured as >400 nm in diameter. (f) Annular dark-field STEM image of a cross section of CTG (N_L = 10, θ_i = 20°). (g) FFT image of the graphene region in (f) (top, left). Inverse FFT image of the STEM image, corresponding to the encircled spots in the FFT pattern (bottom). Schematic of the atomic structures of the CTG (top, right).

Realizing this approach is paramount for the discovery of new properties and the development of devices based on 2D materials.

Here, we report programmed crystal assemblies (PCA) of graphene and monolayer hexagonal boron nitride (ML hBN) films to fabricate high-quality, spatially uniform multilayer films. Two examples are shown to represent the main capabilities of our assembly technique. The first example is a graphene/hBN vertical superlattice, fabricated by alternately stacking graphene and ML hBN to a total number of layers N_L = 5 (Figure 1a). The cross-sectional scanning transmission electron microscopy (STEM) image (Figure 1b) showed five parallel layers with pristine interfaces, with the interlayer spacing d_z = 3.37 Å (Figure S2), which is close to the expected value for graphene and hBN.[17] Electron energy loss spectroscopy (EELS) revealed vertical chemical compositions with alternating C and N peaks along the out-of-plane direction (Figure 1c). Significantly, we observe no additional signals of contaminant elements, such as amorphous hydrocarbon.

The second example is chiral twisted graphite (CTG) with N_L progressively twisting layers around the stacking direction with a constant interlayer rotation θ_i (Figure 1d). A top-down TEM diffraction pattern of a chiral stack with N_L = 6 and θ_i = 10° (Figure 1e) showed diffraction spots with rotational periodicity of ~10°, which indicates angle alignment within ±1°. The atomic structure of a chiral film was directly imaged by cross-sectional STEM on a sample with N_L = 10 and θ_i = 20° (Figure 1f). The graphene layers were visible as 10 bright lines with a constant d_z value of 3.41 Å (Figure S2). Three layers (arrows), separated by $3d_z$, exhibit higher intensity than the surrounding layers and lattice fringes along the in-plane direction. Analysis of a fast Fourier transform (FFT) of the image (Figure 1g) identified that the lattice fringes show a periodicity of 2.15 Å, which corresponds to the graphene lattice constant projected along the armchair $\langle\bar{1}110\rangle$ direction d_x. The vertical three-layer periodicity is expected for the θ_i = 20° stacking configuration: Graphene has 6-fold symmetry and should reach an equivalent orientation every three layers (20°/layer × 3 layers = 60°). The increased intensity may be attributed to electron channelling, which occurs when the electron beam is oriented near a high-symmetry zone axis. Collectively, these results (Figure 1) demonstrate that both chemical compositions and atomic arrangements of van der Waals structures can be controlled at the atomic-level by PCA of graphene and ML hBN crystals.

Our PCA for atomic-scale topography involves four general steps (Figure 2a; details in the Supporting Information): (i) growth of high-quality graphene and ML hBN films with uniform thickness and crystalline orientation on Ge(110) single-crystalline substrates by CVD,[14,18] (ii) mechanical exfoliation of a film (graphene or ML hBN) using thermal release tape after Au superlayer deposition, (iii) placement of exfoliated film on top of another as-grown film at angle θ_i (steps ii and iii are carried out N_L times), and (iv) transfer of stacked film onto a target substrate.

Epitaxial graphene and ML hBN grown on Ge(110) serve as ideal structural-units to realize a scalable and atomically clean assembly process. After optimal growth (Figure S3), graphene and ML hBN showed ML thickness with uniformity >99%, low atomic defects (Figure S4) and single crystallographic orientation across the area of a 2 in. wafer, as confirmed by low-energy electron diffraction (LEED) (Figures 2b and S5). The epitaxial films have straight-edge cuts (Figure S6) with certain crystalline orientations determined by the Ge(110) epi-substrates, which enable control of θ_i without additional characterization of the crystalline structures. Epitaxially grown single-crystalline films, as previously grown on metals, are usually strongly bound to them, so they must be removed by chemical etching to isolate the films. Importantly, the interaction energy between the Ge(110) substrate and the as-grown films is lower than between layered materials,[19] so efficient mechanical exfoliation and stacking can be carried out by exploiting van der Waals interactions without exposing the interfaces to other substances, such as polymer or etchant.[16]

https://doi.org/10.1021/acs.nanolett.1c04139
Nano Lett. XXXX, XXX, XXX−XXX

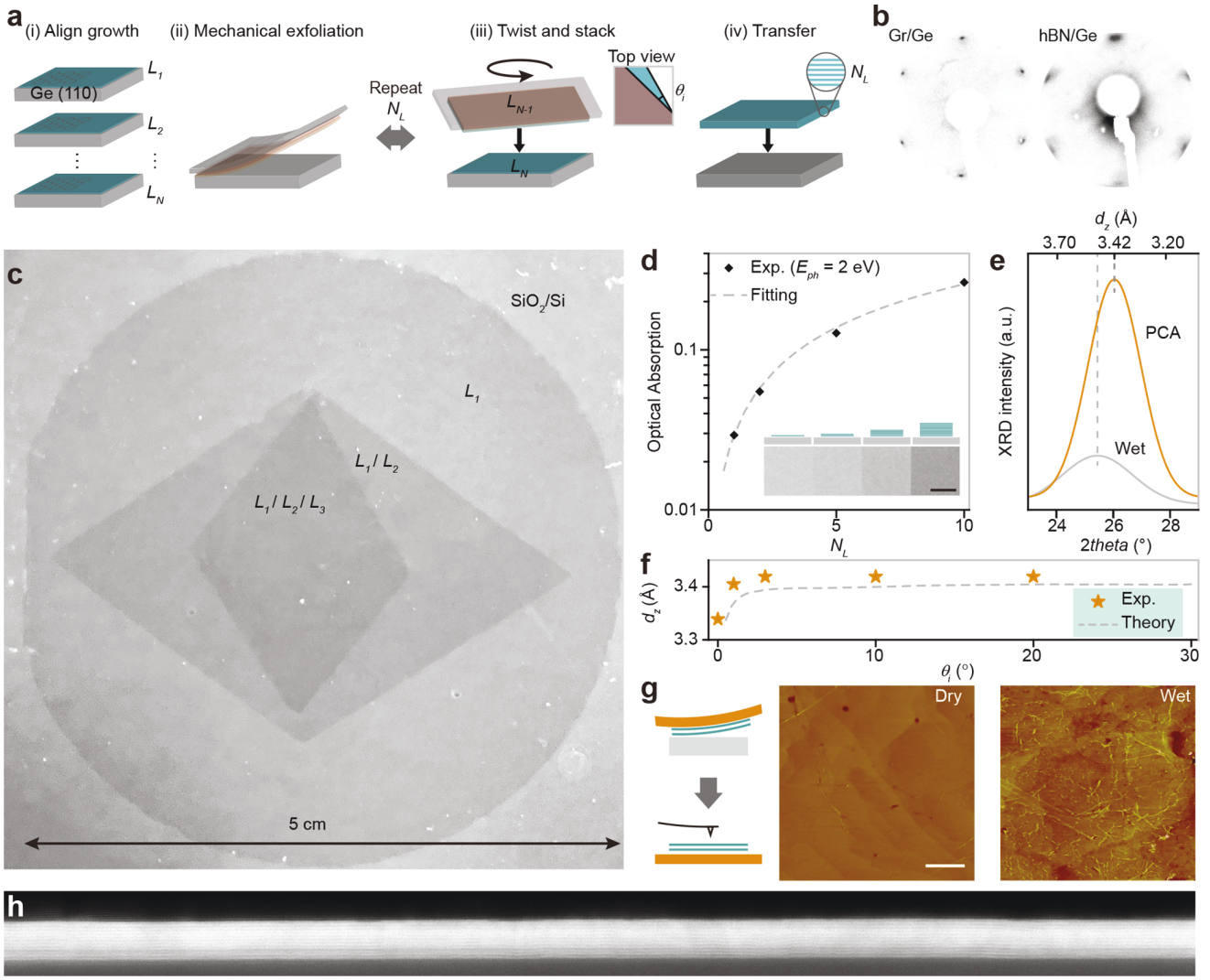

Figure 2. Wafer-scale PCA process for atomic-scale structural engineering. (a) Schematics of the assembly of one-atom-thick crystals, which is conducted in all-dry conditions by exploiting van der Waals interactions. (b) LEED pattern of as-grown graphene (left) and hBN (right) on Ge(110) substrates. (c) Grayscale optical image of wafer-scale, assembled graphene films on a SiO_2/Si substrate. (d) Optical absorption values at 2 eV for films with different N_L, and the expected trend (dashed line) $1 - (T_{SLG})^{N_L}$, where T_{SLG} is the reported transmittance of single-layer graphene. (Inset: optical images of samples with different N_L. Scale bar: 1 mm.) (e) XRD data for films (N_L = 10, θ_i = 20°), prepared by PCA (orange line) and wet-stacking processes (gray line). (f) Measured d_z by XRD in CTG with different θ_i (orange stars) and theoretically predicted values (gray dashed line).[20] (g) Measurement schematics (left) and AFM images of the bottom surfaces of bilayer films, which are prepared by all-dry stacking (center) and wet stacking (right) processes, respectively. The dry stacking sample shows a much flatter surface with fewer wrinkles. (Scale bar: 1 μm, height scale: 50 nm.) (h) Cross-sectional bright-field STEM image of the film in (e) by PCA across 100 nm.

Multilayer films fabricated by the assembly method were uniform over a large-scale. To demonstrate the scalability, wafer-scale graphene films (Figure 2c) were consecutively stacked, and the stacked film was transferred onto a SiO_2/Si substrate. To achieve efficient exfoliation, each film was larger than the one below it. The optical spectra and image (Figures 2d and S7) of the films showed spatially uniform contrasts, which increased linearly as the N_L increased. Near-unity yield of stacking over a macroscopic area was also confirmed by optical absorption measurements in hBN multistacks (Figure S7). The multilayer films offer excellent structural integrity with minimal defects, such as cracks, and therefore yielded suspended films on a holey grid (Figure S8).

The quality of interfaces was investigated in multilayer stacks by conducting out-of-plane X-ray diffraction (XRD) on a millimeter scale. The representative diffraction peak, measured in a CTG with θ_i = 20° and N_L = 10 over a 0.6 cm^2 area (Figure 2e, orange line) showed significantly stronger intensity and lower full width at half maximum than in the reference multilayer film (gray line) prepared by wet transfer. The d_z of 3.42 Å, deduced from the peak position, is consistent with the value measured by direct imaging in STEM (Figures 1f and 2h). On the basis of the Scherrer equation (Supporting Information), the thickness of coherently reflecting lattices is estimated as ~3.6 nm, nearly the value of $(N_L - 1) \times d_z$, which is strong evidence of atomically clean interfaces with uniform d_z across the millimeter-scale sample size. The d_z were also measured for CTG with different θ_i (Figure 2f) to check the reliability of our PCA process for arbitrary twist angle. At θ_i = 0°, d_z was measured as 3.34 Å, which is close to the value for the natural graphite. d_z increased by 2% to 3.42 Å as θ_i increased to 3°, then shows almost constant values for θ_i > 3°.

https://doi.org/10.1021/acs.nanolett.1c04139
Nano Lett. XXXX, XXX, XXX−XXX

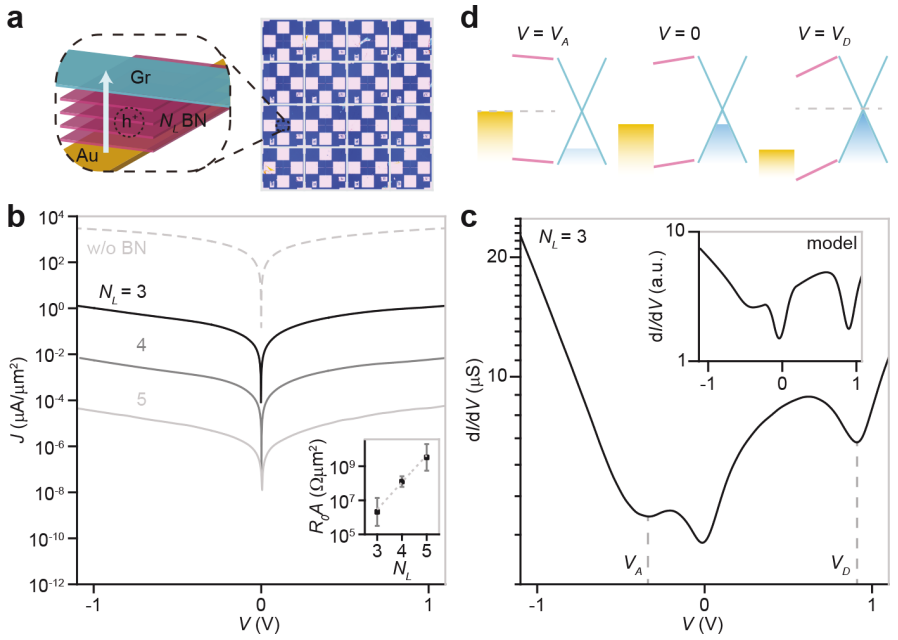

Figure 3. Batch-fabricated tunnel devices. (a) Schematic (left) and optical image (right) of batch-fabricated Gr/hBN/Au tunnel junctions by PCA. (b) J–V curves for hBN tunneling barriers with different N_L. (Inset: N_L-dependent R_0A, averaged from multiple devices with a fitting (dashed line) by a tunneling model.) (c) dI/dV–V curve for N_L = 3. (Inset: Simulated curve with a tunneling model). (d) .

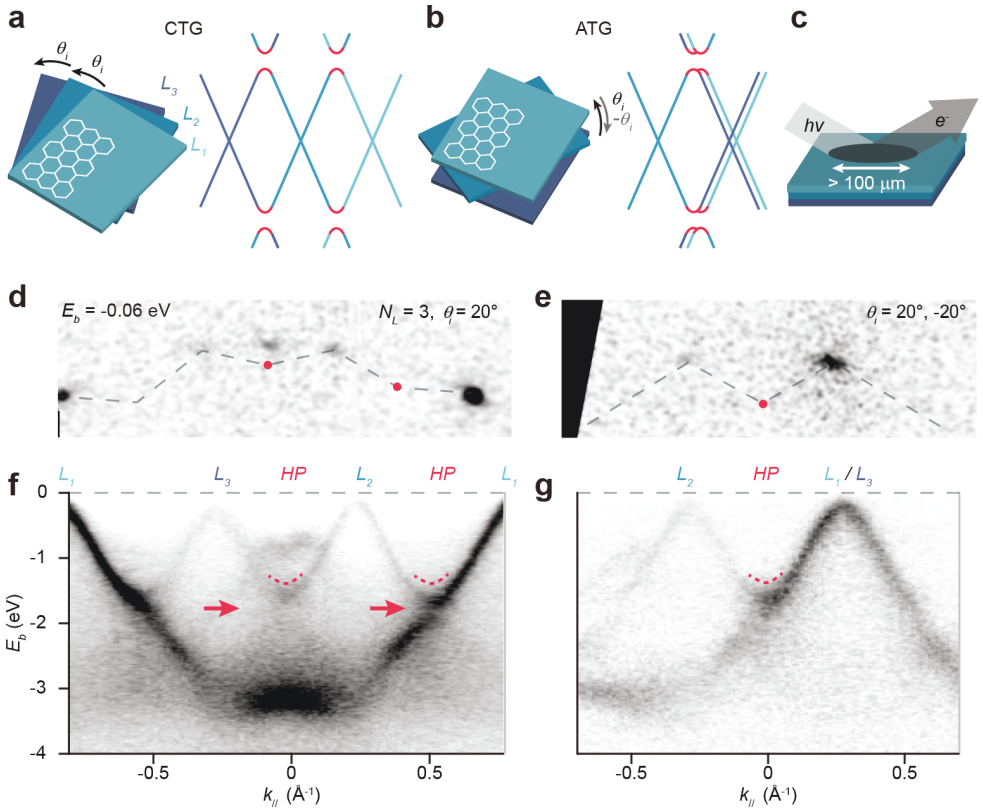

Figure 4. Twisted graphite with programmable electronic band structures. (a, b) Schematics for the stacking configuration and electronic band structures of CTG with a constant rotational polarity (a) and ATG with alternating polarities (b). (c) Schematic for large-scale ARPES measurement. (d, e) Photoemission contours at E_b of −0.06 eV for CTG (N_L = 3, θ_i = 20°; d) and ATG (N_L = 3, θ_i = ± 20°; e). (f, g) Band structures for the CTG (f) and ATG (g) along dashed lines in the contour maps (d) for CTG and (e) for ATG. Dirac cones from the nearest layers form hybridized states at HPs. Parabolic bands (red dotted lines) with minigaps (red arrows) appear at HPs.

This dependence of d_z on θ_i is consistent with a theoretical model (gray line),[20] which considers the structural relaxation by the interlayer interactions. As θ_i increases, the Bernal-stacked regions transform to incommensurate structures with

https://doi.org/10.1021/acs.nanolett.1c04139
Nano Lett. XXXX, XXX, XXX−XXX

high local d_z, so the average d_z increases until the transformation is complete near $\theta_i = 3.3°$.[5] We further examined the cleanliness and surface morphology of multilayers by atomic force microscopy (Figures 2g, S9, and S10), X-ray photoelectron spectroscopy (Figure S10), and optical hyperspectral imaging (Figure S11). Collectively, our results demonstrate that the PCA process forms pristine interfaces.

Our PCA is a powerful tool to generate functional devices, in which atomic-scale control of the structures with pristine interfaces is crucial to obtain desirable properties. We demonstrated the versatility and strength of PCA by producing batch-fabricated tunnel device arrays. They are composed of 2D materials and metallic grids, in which vertical charge transport is strongly affected by interfacial structures such as thickness, atomic defects, and doping of constituent layers.[21] Here, a centimeter-scale graphene film was assembled with hBN of a controlled N_L, then transferred onto gold electrodes to form an array of metal−insulator−metal junctions (Figure 3a). The current densities J normalized by the junction area were measured under ambient conditions. J decreased significantly by ∼1% per layer as N_L increased (Figure 3b). Zero-bias resistance R_0 multiplied by junction area A (Figure 3b, inset) was measured from 22 devices and plotted in the Figure 3b inset. We fit the N_L-dependent R_0A with a basic tunneling equation by taking the barrier height as a free parameter on the assumption that hBN layers have ideal thicknesses with pristine interfaces (Supporting Information). The barrier height was deduced to 3.0 eV for hole-tunneling current; this height is consistent with the energy difference between Fermi level and valence band maximum of hBN on graphite, measured by angle-resolved photoemission spectroscopy (ARPES).[22]

The tunneling current is also determined by the density of states of constituent elements. The plot of differential conductance dI/dV versus the bias voltage V (Figure 3c) shows a dip near the zero-bias region by suppression of phonon-mediated tunneling,[23] plus two local minima at biases of V_A and V_D. Local minima develop when the Fermi level of either electrode is aligned to the Dirac point of graphene that has the minimum density of states (Figures 3d and S12 for confirmation of band alignments). The simulated dI/dV curve (Figure 3c, inset) obtained using a phonon-mediated tunneling model for hole-transports (Figure S13) agrees well with the experimental data; this result confirms the formation of pristine interface with minimized defect-mediated tunneling.

The PCA method also allows scalable and clean integration of various 2D materials, and thereby offers a general approach to design novel van der Waals structures. As an example, the as-grown MoS_2 films were integrated with graphene at near-unity yield to form a uniform graphene/MoS_2 superlattice (Figure S14). The result indicates that all key electronic elements, including metal, semiconductor, and insulator can be assembled with high-quality interfaces on a large-scale. Furthermore, with twist at the pristine interfaces, θ_i-dependent interlayer interactions occur and determine the topology and symmetry of electronic bands.[24] Therefore, θ_i control at multiple interfaces realizes the variety of properties for the given material platform.

We demonstrated a structurally tunable van der Waals platform by fabricating two types of twisted graphite with programmed band topologies (Figure 4a,b) that have a single value of $|\theta_i|$ but different combinations of rotational polarity. Graphene layers stacked with a constant θ_i toward the same rotational polarity produce CTG with periodic electronic bands in the momentum space, hosting equally spaced hybrid states with minigaps by interlayer interactions (Figure 4a, right; red-colored lines). In contrast, stacking of θ_i of alternating sign with an odd N_L forms achiral twisted graphite (ATG) (Figure 4b, left) with a mirror plane in the middle layer. In ATG, the hybrid states of constituent interfaces are superimposed at the same momentum space to interact with each other, so they generate collective states of different topology.[25−28]

ARPES over a large area (100 μm × 300 μm, Figure 4c) revealed the band structures of CTG and ATG ($N_L = 3$, $|\theta_i| = 20°$). Energy-dispersion cross sections were obtained along the multiple Dirac points and hybridization points (HPs, defined in Figure S15) in the momentum space (Figure 4d,e). In CTG (Figure 4f), three equally spaced, conical bands with gradually attenuating intensities formed minigaps at HPs at constant energy (red arrows) and parabolic bands (red dotted lines) (Figures S15−17 for additional data); this result represented hybridization between bands from adjacent layers. In ATG (Figure 4g), the interlayer hybridizations also happened near the crossing point between L_2-band and superimposed L_1/L_3-bands to yield the emergent parabolic band (red dotted line). The confirmation of band structure engineering suggests that PCA can realize the numerous electronic states and correlated properties that have been proposed for ATG[25−28] and CTG[4,29] with effective interlayer interactions across pristine interfaces. Fabrication of twisted multilayer structures with programmed band structures was technically challenging, because even small amounts of contaminants during the stacking can prevent the interlayer interactions. Therefore, most studies on twisted multilayer crystals were conducted in samples with small N_L. Our assembly provides atomically clean interfaces with near-unity yield; therefore, one can reliably program band structures in multilayer films even with large N_L, where various properties are theoretically predicted[28,29] (Figure S18 for chiro-optical property as an example).

Our PCA method can control not only the size but also the atomic shape of the materials to program their intrinsic properties, heralding an exciting era of "nanotopotechnology". Numerous artificial structures can be fabricated by a designer approach with single-atom precision on wafer-scale to study interactions with fundamental elements, facilitating the discovery of various physical properties. For example, van der Waals crystals with controlled interfaces can result in strong infrared photoresponse,[30] ultrathin thermal isolation,[31] enhanced superconductivity,[32] and fast ion diffusions at van der Waals interfaces,[33] which are distinct from natural crystals. In particular, since associated characteristic length scales are very small, such as phonon wavelengths[34] and the radii of interlayer excitons,[35] the properties strongly depend on the interface structures at the atomic scale. Due to the difficulty of forming pristine interfaces, these properties have been demonstrated mostly in samples with a limited number of layers and lateral sizes. Our reliable and scalable method provides a powerful tool for investigating more complex structures and accelerating the development of advanced devices based on van der Waals crystals.

■ ASSOCIATED CONTENT

Supporting Information

The Supporting Information is available free of charge at https://pubs.acs.org/doi/10.1021/acs.nanolett.1c04139.

https://doi.org/10.1021/acs.nanolett.1c04139
Nano Lett. XXXX, XXX, XXX−XXX

Experimental details for growth of 2D materials, PCA and wet process of 2D materials, device fabrication and other characterization tools, discussions of 2D assembly developments, XRD for twisted graphite, ARPES data from trilayer CTG and ATG, circular dichroism for CTG, tunneling model for Gr/hBN/Au tunnel junctions, estimation of tunneling barrier height; figures for summary of 2D assembly developments, cross-sectional STEM, graphene growth, twist angle-controlled stacking, near-unity stacking yield, mechanical robustness of multilayer membrane, surface flatness and cleanliness of multilayer graphene, interlayer optical absorption of twisted bilayer graphene film, Gr/hBN/Au junction devices, graphene/MoS_2 superlattices, band structure of CTG and ATG and chiro-optical properties in CTG (PDF)

AUTHOR INFORMATION

Corresponding Author

Cheol-Joo Kim − *Department of Chemical Engineering, Pohang University of Science and Technology, Pohang, Gyeongbuk 37673, Republic of Korea;* orcid.org/0000-0002-4312-3866; Phone: +82-54-279-5233; Email: kimcj@postech.ac.kr

Authors

Seong-Jun Yang − *Department of Chemical Engineering, Pohang University of Science and Technology, Pohang, Gyeongbuk 37673, Republic of Korea;* orcid.org/0000-0002-7221-0918

Ju-Hyun Jung − *Department of Chemical Engineering, Pohang University of Science and Technology, Pohang, Gyeongbuk 37673, Republic of Korea;* orcid.org/0000-0002-8283-621X

Eunsook Lee − *Beamline Research Division, Pohang Accelerator Laboratory, Pohang, Gyeongbuk 37673, Republic of Korea*

Edmund Han − *Department of Materials Science and Engineering, University of Illinois at Urbana−Champaign, Urbana, Illinois 61801, United States*

Min-Yeong Choi − *Department of Chemical Engineering, Pohang University of Science and Technology, Pohang, Gyeongbuk 37673, Republic of Korea;* orcid.org/0000-0001-6966-3513

Daesung Jung − *Convergence Research Center for Energy and Environmental Sciences, Sungkyunkwan University, Suwon, Gyeonggi 16419, Republic of Korea*

Shinyoung Choi − *Department of Chemical Engineering, Pohang University of Science and Technology, Pohang, Gyeongbuk 37673, Republic of Korea;* orcid.org/0000-0001-5465-7719

Jun-Ho Park − *Department of Chemical Engineering, Pohang University of Science and Technology, Pohang, Gyeongbuk 37673, Republic of Korea;* orcid.org/0000-0003-2887-1994

Dongseok Oh − *Beamline Research Division, Pohang Accelerator Laboratory, Pohang, Gyeongbuk 37673, Republic of Korea*

Siwoo Noh − *Beamline Research Division, Pohang Accelerator Laboratory, Pohang, Gyeongbuk 37673, Republic of Korea*

Ki-Jeong Kim − *Beamline Research Division, Pohang Accelerator Laboratory, Pohang, Gyeongbuk 37673, Republic of Korea;* orcid.org/0000-0001-9233-3096

Pinshane Y. Huang − *Department of Materials Science and Engineering, University of Illinois at Urbana−Champaign, Urbana, Illinois 61801, United States;* orcid.org/0000-0002-1095-1833

Chan-Cuk Hwang − *Beamline Research Division, Pohang Accelerator Laboratory, Pohang, Gyeongbuk 37673, Republic of Korea*

Complete contact information is available at: https://pubs.acs.org/10.1021/acs.nanolett.1c04139

Author Contributions

[⊥]S.-J.Y. and J.-H.J. contributed equally to this work. S.-J.Y. and C.-J.K. designed the experiments. S.-J.Y., J.-H.J., and M.-Y.C. synthesized the 2D films. S.-J.Y. and J.-H.J. conducted the assembly process. E.H. and P.Y.H. carried out atomic-resolution TEM imaging. E.L., D.J., D.O., and C.-C.H. conducted XPS and ARPES measurements. J.-H.J., S.N., and K.-J.K. conducted LEED measurements. S.C. and J.-H.P. carried out hyperspectral imaging. S.-J.Y. and J.-H.J. carried out other sample characterizations. S.-J.Y. and C.-J.K. wrote the manuscript. All authors discussed the results and commented on the manuscript.

Notes

The authors declare no competing financial interest.

ACKNOWLEDGMENTS

This work was supported by the Basic Science Research Program (2020R1C1C1014590), the Basic Research Laboratory Program (2020R1A4A1019455), and the Creative Materials Discovery Program (2018M3D1A1058793 and 2020M3D1A1110548) of the National Research Foundation of Korea (NRF) funded by the Korea government (Ministry of Science and ICT). The electron microscopy work was supported by NSF-MRSEC award no. DMR-1720633, using the Materials Research Laboratory Central Facilities at the University of Illinois, where electron microscopy support was provided by J. Mabon, C. Chen, and H. Zhou. C.-C.H. was supported by the NRF funded by the Ministry of Science and ICT (2020R1A2B5B02001876 and 2018R1A56075964).

REFERENCES

(1) Geim, A. K.; Grigorieva, I. V. Van der Waals heterostructures. *Nature* **2013**, *499*, 419−425.

(2) Kang, K.; Lee, K.-H.; Han, Y.; Gao, H.; Xie, S.; Muller, D. A.; Park, J. Layer-by-layer assembly of two-dimensional materials into wafer-scale heterostructures. *Nature* **2017**, *550*, 229−233.

(3) Kumar, P.; Lynch, J.; Song, B.; Ling, H.; Barrera, F.; Kisslinger, K.; Zhang, H.; Anantharaman, S. B.; Digani, J.; Zhu, H.; Choudhury, T. H.; McAleese, C.; Wang, X.; Conran, B. R.; Whear, O.; Motala, M. J.; Snure, M.; Muratore, C.; Redwing, J. M.; Glavin, N. R.; Stach, E. A.; Davoyan, A. R.; Jariwala, D. Light−matter coupling in large-area van der Waals superlattices. *Nat. Nanotechnol.* **2021**, DOI: 10.1038/s41565-021-01023-x.

(4) Kim, C.-J.; Sánchez-Castillo, A.; Ziegler, Z.; Ogawa, Y.; Noguez, C.; Park, J. Chiral atomically thin films. *Nat. Nanotechnol.* **2016**, *11*, 520−524.

(5) Yoo, H.; Engelke, R.; Carr, S.; Fang, S.; Zhang, K.; Cazeaux, P.; Sung, S. H.; Hovden, R.; Tsen, A. W.; Taniguchi, T.; Watanabe, K.; Yi, G.-C.; Kim, M.; Luskin, M.; Tadmor, E. B.; Kaxiras, E.; Kim, P. Atomic and electronic reconstruction at the van der Waals interface in twisted bilayer graphene. *Nat. Mater.* **2019**, *18*, 448−453.

(6) Cao, Y.; Fatemi, V.; Fang, S.; Watanabe, K.; Taniguchi, T.; Kaxiras, E.; Jarillo-Herrero, P. Unconventional superconductivity in magic-angle graphene superlattices. *Nature* **2018**, *556*, 43−50.

(7) Nam, Y.; Ki, D.-K.; Soler-Delgado, D.; Morpurgo, A. F. A family of finite-temperature electronic phase transitions in graphene multilayers. *Science* **2018**, *362*, 324−328.
(8) Park, J.-H.; Yang, S.-J.; Choi, C.-W.; Choi, S.-Y.; Kim, C.-J. Pristine graphene insertion at the metal/semiconductor interface to minimize metal-induced gap states. *ACS Appl. Mater. Interfaces* **2021**, *13*, 22828−22835.
(9) Kühne, M.; Börrnert, F.; Fecher, S.; Ghorbani-Asl, M.; Biskupek, J.; Samuelis, D.; Krasheninnikov, A. V.; Kaiser, U.; Smet, J. H. Reversible superdense ordering of lithium between two graphene sheets. *Nature* **2018**, *564*, 234−239.
(10) Quan, J.; Linhart, L.; Lin, M.-L.; Lee, D.; Zhu, J.; Wang, C.-Y.; Hsu, W.-T.; Choi, J.; Embley, J.; Young, C.; Taniguchi, T.; Watanabe, K.; Shih, C.-K.; Lai, K.; MacDonald, A. H.; Tan, P.-H.; Libisch, F.; Li, X. Phonon renormalization in reconstructed MoS_2 moiré superlattices. *Nat. Mater.* **2021**, *20*, 1100−1105.
(11) Dai, S.; Ma, Q.; Liu, M. K.; Andersen, T.; Fei, Z.; Goldflam, M. D.; Wagner, M.; Watanabe, K.; Taniguchi, T.; Thiemens, M.; Keilmann, F.; Janssen, G. C. A. M.; Zhu, S.-E.; Jarillo-Herrero, P.; Fogler, M. M.; Basov, D. N. Graphene on hexagonal boron nitride as a tunable hyperbolic metamaterial. *Nat. Nanotechnol.* **2015**, *10*, 682−686.
(12) Wang, L.; Meric, I.; Huang, P. Y.; Gao, Q.; Gao, Y.; Tran, H.; Taniguchi, T.; Watanabe, K.; Campos, L. M.; Muller, D. A.; Guo, J.; Kim, P.; Hone, J.; Shepard, K. L.; Dean, C. R. One-dimensional electrical contact to a two-dimensional material. *Science* **2013**, *342*, 614−617.
(13) Liu, F.; Wu, W.; Bai, Y.; Chae, S. H.; Li, Q.; Wang, J.; Hone, J.; Zhu, X.-Y. Disassembling 2D van der Waals crystals into macroscopic monolayers and reassembling into artificial lattices. *Science* **2020**, *367*, 903−906.
(14) Lee, J.-H.; Lee, E. K.; Joo, W.-J.; Jang, Y.; Kim, B.-S.; Lim, J. Y.; Choi, S.-H.; Ahn, S. J.; Ahn, J. R.; Park, M.-H.; Yang, C.-W.; Choi, B. L.; Hwang, S.-W.; Whang, D. Wafer-scale growth of single-crystal monolayer graphene on reusable hydrogen-terminated germanium. *Science* **2014**, *344*, 286−289.
(15) Lee, J. S.; Choi, S. H.; Yun, S. J.; Kim, Y. I.; Boandoh, S.; Park, J.-H.; Shin, B. G.; Ko, H.; Lee, S. H.; Kim, Y.-M.; Lee, Y. H.; Kim, K. K.; Kim, S. M. Wafer-scale single-crystal hexagonal boron nitride film via self-collimated grain formation. *Science* **2018**, *362*, 817−821.
(16) Lin, Y.-C.; Lu, C.-C.; Yeh, C.-H.; Jin, C.; Suenaga, K.; Chiu, P.-W. Graphene annealing: How clean can it be? *Nano Lett.* **2012**, *12*, 414−419.
(17) Giovannetti, G.; Khomyakov, P. A.; Brocks, G.; Kelly, P. J.; van den Brink, J. Substrate-induced band gap in graphene on hexagonal boron nitride: *Ab initio* density functional calculations. *Phys. Rev. B* **2007**, *76*, No. 073103.
(18) Yin, J.; Liu, X.; Lu, W.; Li, J.; Cao, Y.; Li, Y.; Xu, Y.; Li, X.; Zhou, J.; Jin, C.; Guo, W. Aligned growth of hexagonal boron nitride monolayer on germanium. *Small* **2015**, *11*, 5375−5380.
(19) Yang, S.-J.; Choi, S.; Odongo Ngome, F. O.; Kim, K.-J.; Choi, S.-Y.; Kim, C.-J. All-dry transfer of graphene film by van der Waals interactions. *Nano Lett.* **2019**, *19*, 3590−3596.
(20) Wijk, M. M. v.; Schuring, A.; Katsnelson, M. I.; Fasolino, A. Relaxation of moiré patterns for slightly misaligned identical lattices: graphene on graphite. *2D Mater.* **2015**, *2*, No. 034010.
(21) Britnell, L.; Gorbachev, R. V.; Jalil, R.; Belle, B. D.; Schedin, F.; Mishchenko, A.; Georgiou, T.; Katsnelson, M. I.; Eaves, L.; Morozov, S. V.; Peres, N. M. R.; Leist, J.; Geim, A. K.; Novoselov, K. S.; Ponomarenko, L. A. Field-effect tunnelling transistor based on vertical graphene heterostructures. *Science* **2012**, *335*, 947−950.
(22) Pierucci, D.; Zribi, J.; Henck, H.; Chaste, J.; Silly, M. G.; Bertran, F.; Le Fevre, P.; Gil, B.; Summerfield, A.; Beton, P. H.; et al. Van der Waals epitaxy of two-dimensional single-layer h-BN on graphite by molecular beam epitaxy: Electronic properties and band structure. *Appl. Phys. Lett.* **2018**, *112*, 253102.
(23) Zhang, Y.; Brar, V. W.; Wang, F.; Girit, C.; Yayon, Y.; Panlasigui, M.; Zettl, A.; Crommie, M. F. Giant phonon-induced conductance in scanning tunnelling spectroscopy of gate-tunable graphene. *Nat. Phys.* **2008**, *4*, 627−630.
(24) Pal, A.; Mele, E. J. Nodal surfaces in photoemission from twisted bilayer graphene. *Phys. Rev. B* **2013**, *87*, 205444.
(25) Carr, S.; Li, C.; Zhu, Z.; Kaxiras, E.; Sachdev, S.; Kruchkov, A. Ultraheavy and ultrarelativistic dirac quasiparticles in sandwiched graphenes. *Nano Lett.* **2020**, *20*, 3030−3038.
(26) Hao, Z.; Zimmerman, A. M.; Ledwith, P.; Khalaf, E.; Najafabadi, D. H.; Watanabe, K.; Taniguchi, T.; Vishwanath, A.; Kim, P. Electric field-tunable superconductivity in alternating-twist magic-angle trilayer graphene. *Science* **2021**, *371*, 1133−1138.
(27) Park, J. M.; Cao, Y.; Watanabe, K.; Taniguchi, T.; Jarillo-Herrero, P. Tunable strongly coupled superconductivity in magic-angle twisted trilayer graphene. *Nature* **2021**, *590*, 249−255.
(28) Khalaf, E.; Kruchkov, A. J.; Tarnopolsky, G.; Vishwanath, A. Magic angle hierarchy in twisted graphene multilayers. *Phys. Rev. B* **2019**, *100*, No. 085109.
(29) Wu, F.; Zhang, R.-X.; Das Sarma, S. Three-dimensional topological twistronics. *Phys. Rev. Res.* **2020**, *2*, No. 022010.
(30) Deng, B.; Ma, C.; Wang, Q.; Yuan, S.; Watanabe, K.; Taniguchi, T.; Zhang, F.; Xia, F. Strong mid-infrared photoresponse in small-twist-angle bilayer graphene. *Nat. Photonics* **2020**, *14*, 549−553.
(31) Kim, S. E.; Mujid, F.; Rai, A.; Eriksson, F.; Suh, J.; Poddar, P.; Ray, A.; Park, C.; Fransson, E.; Zhong, Y.; Muller, D. A.; Erhart, P.; Cahill, D. G.; Park, J. Extremely anisotropic van der Waals thermal conductors. *Nature* **2021**, *597*, 660−665.
(32) Arora, H. S.; Polski, R.; Zhang, Y.; Thomson, A.; Choi, Y.; Kim, H.; Lin, Z.; Wilson, I. Z.; Xu, X.; Chu, J.-H.; Watanabe, K.; Taniguchi, T.; Alicea, J.; Nadj-Perge, S. Superconductivity in metallic twisted bilayer graphene stabilized by WSe_2. *Nature* **2020**, *583*, 379−384.
(33) Kühne, M.; Paolucci, F.; Popovic, J.; Ostrovsky, P. M.; Maier, J.; Smet, J. H. Ultrafast lithium diffusion in bilayer graphene. *Nat. Nanotechnol.* **2017**, *12*, 895−900.
(34) Vaziri, S.; Yalon, E.; Muñoz Rojo, M.; Suryavanshi, S. V.; Zhang, H.; McClellan, C. J.; Bailey, C. S.; Smithe, K. K. H.; Gabourie, A. J.; Chen, V.; et al. Ultrahigh thermal isolation across heterogeneously layered two-dimensional materials. *Sci. Adv.* **2019**, *5*, No. eaax1325.
(35) Fang, H.; Battaglia, C.; Carraro, C.; Nemsak, S.; Ozdol, B.; Kang, J. S.; Bechtel, H. A.; Desai, S. B.; Kronast, F.; Unal, A. A.; Conti, G.; Conlon, C.; Palsson, G. K.; Martin, M. C.; Minor, A. M.; Fadley, C. S.; Yablonovitch, E.; Maboudian, R.; Javey, A. Strong interlayer coupling in van der Waals heterostructures built from single-layer chalcogenides. *Proc. Natl. Acad. Sci. U. S. A.* **2014**, *111*, 6198−6202.

https://doi.org/10.1021/acs.nanolett.1c04139
Nano Lett. XXXX, XXX, XXX−XXX